2019

Modern laser speckle contrast theory: flaws and consequences

BOSTON UNIVERSITY

COLLEGE OF ENGINEERING

Thesis

MODERN LASER SPECKLE CONTRAST THEORY: FLAWS AND CONSEQUENCES

by

CHANG LIU

B.S. Southern Medical University

Submitted in partial fulfillment of the

requirements for the degree of

Master of Science

2019

Approved by

First Reader

David A. Boas, PhD
Professor of Biomedical Engineering
Professor of Electrical and Computer Engineering

Second Reader

Darren Roblyer, PhD
Assistant Professor of Biomedical Engineering

Third Reader

Dmitry D. Postnov, PhD
Postdoctoral Fellow

Dedication

I would like to dedicate this work to my families, who have always been standing by my side, understanding me, and supporting me. It wouldn't happen without their continuous love!

Acknowledgments

First of all, I would like to express my sincere gratitude to my advisor Prof. David Boas, for providing the original idea of the research and helping me go through it. It is very grateful to have the opportunity to work in the "BOAS" Lab at Boston University, which opened my mind on optical imaging and motivated me all the time.

Second, I want to thank Dr. Dmitry Postnov. His guidance helped me in all the time of my research, thesis writing and the methodology of scientific research. He is the best mentor ever!

Finally, I would like to thank all "BOAS Lab" members, for their help in both research and life. Love to everyone!

MODERN LASER SPECKLE CONTRAST THEORY: FLAWS AND CONSEQUENCES

CHANG LIU

ABSTRACT

Laser speckle contrast imaging (LSCI) is a non-invasive optical imaging technique for monitoring blood flow in brain, skin, and retina. The simple and cheap instrument make it a promising technology for both clinical applications and research. Modern LSCI theory takes advantage of the relation between blood flow and the speckle contrast $v \propto 1/K^2$ to provide a online acquisition of a full-field blood flow image. However, the assumptions about the form of field correlation function, static scattering effect, and the coherence factor make interpretation of the contrast imprecise. Here we examined how the assumptions in modern LSCI theory affect the relative blood flow measurement and utilized Dynamic Laser Speckle Imaging (DLSI) to validate the imprecision of modern LSCI. Most importantly, the contrast models for measuring relative flow in brain parenchyma and the large vessels were derived. It turns out that modern LSCI underestimates blood flow change and leads to significant error for slow blood flow measurement.

Contents

List of Tables

List of Figures

List of Abbreviations

CBF	.....	Cerebral Blood Flow
$CMRO_2$	.....	Cerebral metabolic rate of oxygen
DCS	.....	Diffusion correlation spectroscopy
DLSI	.....	Dynamic Laser Speckle Imaging
LDF	.....	Laser Doppler Flowmetry
LDI	.....	Laser Doppler Imaging
LSCI	.....	Laser Speckle Contrast Imaging
$MU_{n=0.5}$	.....	Multiple scattering & unordered motion
$MO/SU_{n=1}$	.....	Multiple scattering & ordered motion
	.....	or single scattering & unordered motion
OCT	.....	Optical Coherence Tomography
rCBF	.....	relative Cerebral Blood Flow
RE	.....	Relative Error
ROI	.....	Region of interest
$SO_{n=2}$	.....	Single scattering & ordered motion

Chapter 1

Introduction

Cerebral blood flow (CBF) functions as a carrier to provide oxygen, glucose and other nutrition to brain tissue, for maintaining the normal brain function. The lack of brain blood would damage the tissue and cause neurological diseases. In neuropathology, measurement of cerebral blood flow benefits disease diagnosis and treatment. CBF measurement techniques include magnetic resonance imaging (MRI), positron emission tomography (PET), single-photon-emission computed tomography (SPECT) have been widely applied in clinics. These techniques are disadvantaged by the low spatial resolution and their disability of continuous CBF monitor. Recently, various optical techniques are developed and are promising in online CBF monitor.

1.1 Laser Doppler flowmetry and Laser Doppler Imaging

Laser Doppler flowmetry (LDF) makes use of the Doppler shift after the light interacts with the moving red blood cells. The Doppler-shifted light interferes with the light scattered from the stationary part to form the temporal fluctuating speckle pattern. A probe is used to detect the temporal variation of the scattered light intensity at every single point to calculate the frequency shift of the scattered light. The blood perfusion in LDF is defined as the product of the concentration of the red blood cells and their average speed and can be derived from the Doppler power spectrum of the frequency-shifted light (Fredriksson et al., 2007). LDF has been utilized in continuous cerebral blood flow measurement in rats (Dirnagl et al., 1989; Dunn et al., 2001).

Currently, two types of commercial LDF devices are available for blood perfusion measurement: Laser Doppler perfusion monitor (LDPM) and Laser Doppler perfusion imaging (LDPI). LDPM detects the temporal changes of the light intensity of a small sampling region while LDPI allows a two-dimensional perfusion map by scanning. The use of probe and scanning limits the spatial measurement and the speed of LDF. The Development of the fast-speed CMOS image sensor triggers the emergence of Laser Doppler Imaging technique (LDI) which enables the real-time full-field CBF measurement (Serov and Lasser, 2005).

1.2 Diffusion correlation spectroscopy

Diffusion correlation spectroscopy (DCS) is a non-invasive optical technique that has been used in relative cerebral blood flow (rCBF) measurement of animals and human brain (Buckley et al., 2014). The technique measures the temporal fluctuation of the near-infrared light scattererd from the moving red blood cells. The measured intensity autocorrelation function is fitted with the photon diffusion model to obtain cerebral blood flow index (CBFi, cm^2/s) (Durduran and Yodh, 2014). The rCBF measured by DCS has been validated by the traditional clinical CBF measure technique arterial-spin labeled MRI (ALS-MRI). As an inexpensive and portable technique, DCS has been used in both intensive care unit (ICU) and operating room (OR), and is particular popular in CBF monitor of infants and young children. Recent studies combine DCS with NIR spectroscopy to obtain the cerebral blood flow and the cerebral metabolic rate of oxygen ($CMRO_2$). Like all optical techniques, DCS is limited by the superficial measurement depth and the sensitivity of motion. And it is still a challenge for DCS to achieve deep cerebral blood flow measurement.

1.3 Laser speckle contrast imaging

Laser speckle contrast imaging (LSCI) is a non-invasive optical technique for monitoring blood flow in skin (Huang et al., 2008; Choi et al., 2004; Roustit et al., 2010), retina (Briers and Webster, 1996; Srienc et al., 2010), and brain (Dunn et al., 2001; Shin et al., 2006; Nakamura et al., 2010). It has been recently approved by American Food and Drug Association as a medical device for retinal blood flow monitor. Laser light shined into the detected object is back-scattered and is collected using a CCD camera, which gives rise to a speckle image. The speckle image is post-processed through the computer system to obtain the contrast image and finally display the blood flow map. LSCI provides online full-field blood flow image with high spatial and temporal resolution. Figure 1·1 shows the image setup of LSCI and the example of the speckle contrast image and the blood flow map.

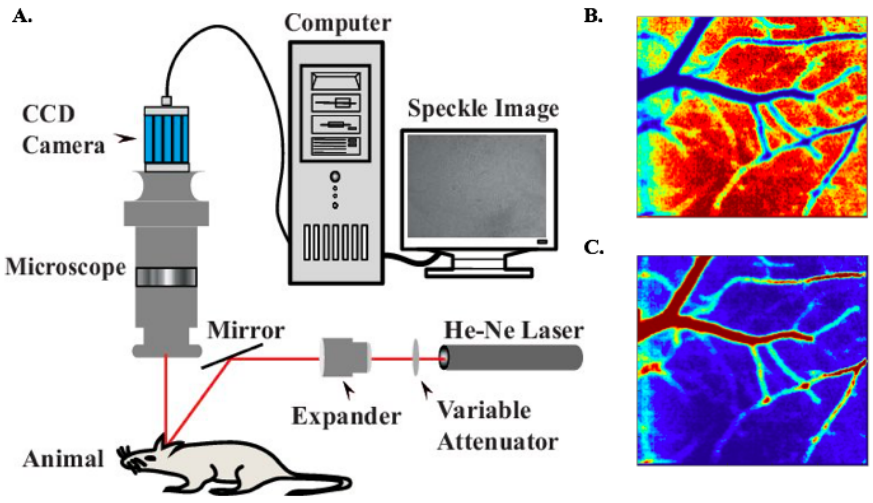

Figure 1·1: (A) A typical LSCI setup (Qiu et al., 2010). (B) Speckle contrast image and (C) blood flow map of a region of interest in a mouse brain during normal condition.

However, LSCI is limited by the imprecision contrast model it used to calculate relative blood flow, which prevents it from becoming a quantitative imaging tech-

nique. The imprecision of the speckle contrast model originates from the unclear knowledge about how light interacts with the tissue and vessels. Many studies had pointed out the problems and the limitations of modern laser speckle contrast theory (Boas and Dunn, 2010; Duncan and Kirkpatrick, 2008; Senarathna et al., 2013). At the same time, measurement deviation had been observed between the blood flow results obtained by LSCI and other techniques. Table 1 gives an example of the discrepancy between rCBF in brain parenchyma obtained by LSCI and optical coherence tomography (OCT) that was observed in the BOAS group.

Experiment	Baseline	1 hour ischemia	1 hour reperfusion
Laser speckle		41%	74%
OCT CBF arterial ($ml/min/mm^2$)	2.5×10^{-4}	1.2×10^{-5} (4.7%)	1.6×10^{-4} (66.2%)

Table 1.1: rCBF (% of baseline) measured by LSCI and OCT in mouse brain parenchyma during normal condition, 1 hour after middle cerebral artery occlusion and reperfusion. Data by Evren Erdener, BOAS group, Boston University, 2017.

From the table, obvious measurement deviation can be observed for rCBF one hour after ischemia: the rCBF measured by LSCI is 41% of baseline, whereas the rCBF measured by OCT is 4.7% of baseline. The deviation might result from the flaws in modern LSCI theory. We hypothesize that modern LSCI measurement underestimates blood flow change.

The speckle contrast model currently used in LSCI gives rise to the result that $v \propto 1/K^2$, so that the blood flow can be easily derived from the square of the reciprocal of the contrast. This "simplified contrast model" is based on assumptions about the form of field correlation function, static scattering effect, and the coherence factor. In this study, we aim to test the imprecision of the modern laser speckle contrast imaging for CBF measurement during normal condition and pathological

conditions, to find out how these theoretical assumptions affect the cerebral blood flow measurement.

Chapter 2

Principles of Modern Laser speckle contrast theory

2.1 Speckle pattern formation

In optical physics, when illuminating coherence light (e.g. laser light) into a scattering object, the light passes through the object and interacts with the scatterers inside. Depending on the physical properties of the scatterers (e.g. shape, scattering coefficient etc.), a portion of the light are back-scattered from the scatterers. Due to the various trajectories, the back-scattered light interfere with each other constructively or destructively, generating a speckle pattern with randomly varied intensity (Figure 2·1).

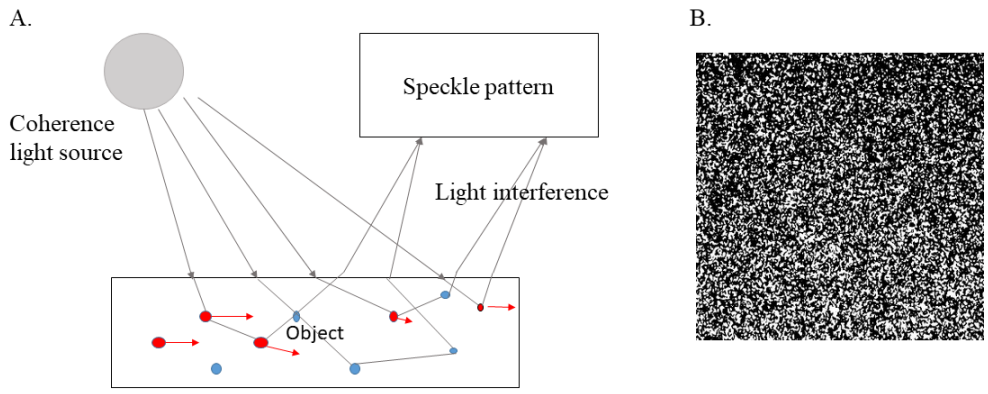

Figure 2·1: (A) Speckle pattern formation. The light back-scattered from the moving particles (red) and the static particles (blue) interfere to form the speckle pattern. (B) An example of laser speckle pattern (Briers, 2001).

2.2 Speckle dynamics

The dynamics of the speckle pattern are closely linked to the movement of the scatterers: fixed scatterers form a static speckle pattern, whose intensity remains the same along time; moving scatterers generate a dynamic speckle pattern with the intensity temporally fluctuating. As the speckle pattern fluctuates according to the scatterers movement, it is natural to relate the speckle dynamics with the movement information of the scatterers (e.g., velocity or displacement). Therefore, there is a necessity to describe the speckle dynamics quantitatively. Currently, three physical characteristics have been brought up to describe the speckle dynamics: the field correlation function, the intensity correlation function, and the speckle contrast.

2.2.1 Field correlation function

The movement of the scatterers causes the fluctuation of the electric field of back-scattered light. The dynamics of the electric field can be quantified using the field correlation function, which is represented as follows:

$$g_1(\tau) = \frac{< E(t)E^*(t+\tau) >_t}{< E(t)E^*(t) >_t} \tag{2.1}$$

τ is the time lag. $< ... >$ indicates ensemble average that can be approximated by time average when assuming ergodic system. As the electric field fluctuates over time, the speckle pattern decorrelates and the $g_1(\tau)$ function decays. The time it takes for the field correlation function to decay to a specific value where the speckle patterns are decorrelated is called the "correlation time (τ_c)". The reciprocal of the correlation time is inversely proportional to the particle speed. How fast the field correlation function decays is determined by the particle movement: the faster particle moves, the faster the field correlation function decays, and the shorter correlation time τ_c is.

In reality, it is hard to measure the field correlation function directly, hence the intensity correlation function was introduced.

2.2.2 Intensity correlation function

Intensity correlation function describes the correlation of the scattering intensity, providing a quantitative measurement of the speckle dynamics. The definition of the function is:

$$g_2(\tau) = \frac{< I(t)I(t+\tau) >_t}{< I(t) >_t^2} \tag{2.2}$$

τ is the time lag. The intensity correlation function computes the intensity correlation between time t and $t+\tau$. The value is usually between one and two. A fast decay of the intensity correlation function indicates a high rate of change of the intensity and a fast movement. To measure $g_2(\tau)$, multiple frames of images are needed before the

speckle pattern decorrelates, thus a high-speed camera is required.

The intensity correlation function provides a measurable method to quantify the speckle dynamics. It can be linked to the field correlation function via Siegert relation:

$$g_2(\tau) = 1 + \beta|g_1(\tau)|^2 \tag{2.3}$$

$\beta \leq 1$ is the coherence factor decided by the optical system (Lemieux and Durian, 1999). As a result, a bridge between the intensity correlation function and the particle movement is built up.

2.3 Speckle contrast

2.3.1 Spatial speckle contrast

In the 1980s, Briers and Fercher first used the spatial speckle contrast to quantify the speckle dynamics in the retina. The contrast value is related to the correlation time through laser speckle contrast analysis (LASCA) to obtain a full-field map of retinal blood flow (Briers and Webster, 1996). The spatial speckle contrast K is defined as the ratio of the standard deviation to the mean intensity:

$$K_s = \frac{\sigma_s}{< I >} \tag{2.4}$$

Where σ_s is the spatial standard deviation of the local intensity, and $< I >$ is the local mean value. The contrast value remains high when the speckle pattern is static and reduces when the speckle pattern blurred due to the particle movement. Local standard deviation and the mean intensity are calculated within a window of 7×7 or 5×5 pixels to obtain the spatial speckle contrast via Eq. (2.4). The spatial speckle contrast analysis describes the speckle dynamics with high temporal resolution, typically in the scale of milliseconds. However, due to the local computation, the spatial contrast image is smaller than the original speckle image and the spatial resolution

is lost to some extent. Figure 2·2 depicts the spatial contrast data processing.

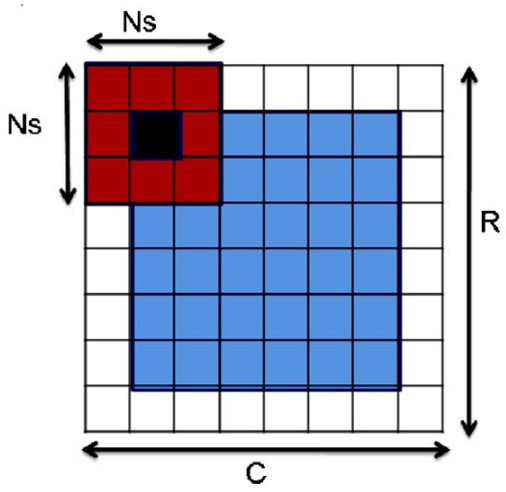

Figure 2·2: Spatial contrast calculation. Local contrast is calculated within the red window ($N_s \times N_s$ pixels). The blue image is the final obtained spatial contrast image (Ansari and Nirala, 2015).

2.3.2 Temporal speckle contrast

Another method to calculate the speckle contrast is through the temporal statistics of the time-integrated speckle image (Cheng et al., 2003). The definition of the temporal speckle contrast K_t has the same form as Eq. (2.4), but it calculates the temporal standard deviation and the mean of intensity within a temporal window. The temporal window is suggested at least 15 frames. Figure 2·3 illustrates how temporal contrast is obtained.

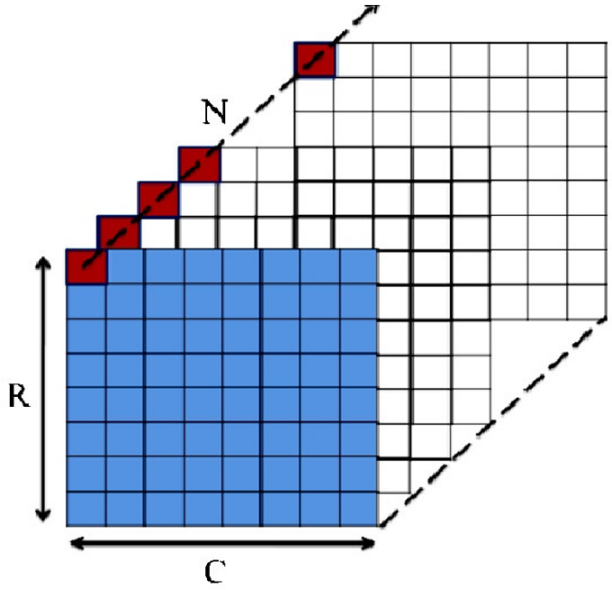

Figure 2·3: Temporal contrast calculation. Temporal contrast of the red pixel is calculated in the time scale using N frames of the speckle image. The blue image is the final temporal contrast image (Ansari and Nirala, 2015).

The method enhanced the spatial resolution but at the lose of the temporal resolution.

2.3.3 Computational realization and simplified analysis

The speckle contrast is related to the speckle variance and can be represented by the autocovariance function as (Briers and Webster, 1996; Bandyopadhyay et al., 2005):

$$K^2 = \frac{\sigma_s^2(T)}{< I >^2} = \frac{2}{T < I >^2} \int_0^T (1 - \frac{\tau}{T}) C_t(\tau) d\tau \tag{2.5}$$

where T is the exposure time, σ_s^2 is the spatial speckle variance, $C_t(\tau)$ is the autocovariance function defined as:

$$C_t(\tau) =< [I(t) - < I(t) >_t][I(t+\tau) - < I(t) >_t] >_t \tag{2.6}$$

The autocovariance $C_t(\tau)$ can be represented by the intensity correlation function g_2:

$$g_2(\tau) = 1 + \frac{C_t(\tau)}{< I >_t^2} \tag{2.7}$$

The intensity correlation function is linked to the field correlation function through the Siegert relation Eq. (2.3). Assuming single light scattering and unordered particle motion, the field correlation function is treated as an exponential decay:

$$g_1(\tau) = exp(-\tau/\tau_c) \tag{2.8}$$

where τ_c, the correlation time, is the time takes for the field correlation function to drop to $1/e$. As a result, we have the spatial speckle contrast as a function of the correlation time τ_c, the coherence factor β, and the exposure time T. :

$$K = \beta^{1/2}\left\{\frac{\tau_c}{T} + \frac{\tau_c^2}{2T^2}\Big[exp\Big(-\frac{2T}{\tau_c}\Big) - 1\Big]\right\}^{1/2} \tag{2.9}$$

Using Eq. (2.9) to calculate correlation time from the observed speckle contrast is computationally expensive. In the original application of LSCI on retinal blood flow measurement, the order of magnitude of the correlation time is on the scale of microseconds, which is much shorter than the exposure time (typical between 0 and $10ms$). Hence the second-moment term in Eq. (2.9) is negligible, giving rise to the simplified speckle contrast equation (Cheng and Duong, 2007):

$$K = \beta^{1/2}\Big(\frac{\tau_c}{T}\Big)^{1/2} \tag{2.10}$$

The simplified contrast model indicates that the correlation time is proportional to the speckle contrast. With the conclusion from dynamic light scattering, the blood flow become inversely proportional to the square of speckle contrast:

$$V \propto 1/K^2 \tag{2.11}$$

In the perspective of disease diagnosis, people pay more attention to the relative value of the blood flow which is closely tied with diseases such as stroke. With the simplified contrast model Eq. (2.11), the relative flow can be easily obtained through the ratio between the K^2 at baseline and the response. The simplified LSCI model improves the efficiency of data processing and accomplishes real-time monitor of blood flow. It has become the most commonly used model in modern LSCI for retinal blood flow monitor (Srienc et al., 2010)and cerebral blood flow measurement (Hecht et al., 2016; Liu et al., 2018; Liu et al., 2011; Li et al., 2013).

Chapter 3

Principal assumptions in LSCI

3.1 Correlation time is short

The assumption of the relation between the correlation time and the exposure time is essential for the simplification of the contrast model.

In visible vessels, the correlation time is on the scale of hundreds of microseconds, while the typical value of the exposure time used for LSCI measurement in cerebral blood flow is $5ms$ (Yuan et al., 2005). Hence the correlation time is much shorter than the exposure time, and the complete speckle contrast model Eq.(2.9) can be replaced by its simplified form Eq. (2.10). However, for slow blood flow in arterioles and capillaries at brain parenchyma and the reduced blood flow during pathological conditions such as stroke, the correlation time can be several milliseconds. In these cases, the assumption $\tau_c << T$ is broken and applying the simplified speckle contrast model would cause measurement error.

3.2 Spatial averaging and Coherence factor β

In LSCI, proper analysis of the speckle statistics is of extreme importance as it directly impacts the calculation of the speckle contrast. The estimation of speckle contrast K is closely dependent on how detector samples the speckle pattern: the spatial averaging effect. Based on the Nyquist theorem, the speckle size should be at least twice larger than the pixel size. The minimum speckle size is determined by the

optical system:

$$\rho_{speckle} = 2.44\lambda(1+M)f/_{\#} \tag{3.1}$$

M is the magnification of the system, λ is the wavelength of light, and $f/_{\#}$ is the f number of the system. In modern LSCI, the speckle size is matched with the pixel size, which undersamples the speckle pattern and might lead to spatial averaging of the uncorrelated speckles. Succeeding study demonstrated the match between speckle size and pixel size caused contrast reduction. (Kirkpatrick et al., 2008).

The coherence factor β from Siegert relation was used to account for the spatial averaging effect in LSCI. β can be obtained by computing the global contrast of a static speckle image. Since the object is not moving, the correlation time τ_c is infinitely close to the exposure time and the global contrast is equal to the square root of the coherence factor:

$$K = \sqrt{\beta} \tag{3.2}$$

However, β was assumed as one in Fercher and Briers's original contrast equation (Fercher and Briers, 1981), which is only the truth under certain situations (Bandyopadhyay et al., 2005). In practice, there is a need to measure β before each individual experiment to make reproducible quantitative connection between the speckle contrast and the blood flow.

3.3 Static scattering effect

LSCI collects the light that is back-scattered from the object to obtain the speckle image. The light scattered from moving scatterers (e.g., red blood cells) contributes to the fluctuations of the speckle pattern while the light scattered from the static scatterers generates the frozen background. However, this effect is ignored in modern LSCI theory, causing the underestimation of the speckle contrast (Boas and Dunn, 2010). multi-exposure speckle imaging (MESI) was designed to measure blood flow

with the presence of static scattering (Parthasarathy et al., 2008). Dynamic component ρ was introduced to describe the static scattering effect of the speckle pattern, the definition of dynamic component is the ratio of the mean intensity of the light back-scattered from the dynamic scatterer (I_f) to the mean intensity of the total back-scattered light:

$$\rho = \frac{< I_f >}{< I_f > + < I_s >} \tag{3.3}$$

$< I_s >$ is the mean intensity of the light back-scattered from the static scatterers. With the static scattering under consideration, the Siegert relation is modified as:

$$g_2(\tau) = 1 + \beta\big[\rho^2 |g_{1,f}(\tau)|^2 + 2\rho(1-\rho)|g_{1,f}(\tau)| + (1-\rho)^2\big] \tag{3.4}$$

Assuming the first-order field correlation function Eq. (8), the improved speckle contrast equation is:

$$K = \beta^{1/2}\left\{\rho^2 \frac{e^{-2x} - 1 + 2x}{2x^2} + 4\rho(1-\rho)\frac{e^{-x} - 1 + x}{x^2} + (1-\rho)^2\right\}^{1/2} \tag{3.5}$$

where $x = T/\tau_c$.

In MESI, the speckle contrasts are obtained with different exposure times. The contrast versus exposure time curve is fitted using Eq. (3.5) to approximate the correlation time τ_c, the dynamic component ρ, and the coherence factor β. This method allows a more precise blood flow measurement with the static scattering effect considered.

3.4 Form of the field correlation function (the most critical assumption)

Since the first study of the laser speckle contrast theory, the exponentially decaying form of field correlation function Eq. (2.8) was assumed for contrast equation derivation. However, according to the dynamic light scattering, the form of the field

correlation function is determined by the scattering regime and the particle movement (Bandyopadhyay et al., 2005; Davis et al., 2016). Table 3.1 shows three forms of the field correlation function: the exponential form is appropriate to single scattering & unordered motion and multiple scattering & ordered motion; $exp(-\sqrt{\tau/\tau_c})$ is proper for multiple scattering & unordered motion; the Gaussian-shaped field correlation function $exp[-(\tau/\tau_c)^2]$ is correct for single scattering & ordered motion.

g_1 model	Light scattering	Movement type	Notation
$exp(-\sqrt{\tau/\tau_c})$	Multiple scattering	Unordered	$MU_{n=0.5}$
$exp(-\tau/\tau_c)$	Multiple scattering	Orderd	$MO/SU_{n=1}$
	Single scattering	Unordered	
$exp[-(\tau/\tau_c)^2]$	Single scattering	Ordered	$SO_{n=2}$

Table 3.1: Field correlation function in terms of the scattering regime and the particle motion. τ_c is the correlation time.

The corresponding contrast equation of the Gaussian-shaped field correlation function had been derived (Duncan and Kirkpatrick, 2008). However, at the early stage, the application of LSCI focused on blood flow measurement in large retinal vessels, in which the blood flow is fast and the correlation time τ_c is much shorter than the exposure time T. A comparison of the two contrast models with exponential decay form and the Gaussian-shaped field correlation function found out that the speckle contrasts estimated by two contrast models are identical when $\tau_c << T$ (Ramirez-San-Juan et al., 2008). Consequently, only the speckle contrast equation with the exponentially decay field correlation function was widely used in LSCI due to its simple form.

However, single scattering almost never the case. For LSCI measurement in capillaries and arterioles of which the vessel sizes are smaller as compared to the photon

mean free path, most back-scattered photons are scattered multiple times (Davis et al., 2014; Kazmi et al., 2015). Besides, particles in blood vessels are not all featured by unordered motion.

Recent study in BOAS group (Postnov et al., 2019) uncovered that multiple scattering & unordered motion dominants in brain parenchyma, and single scattering & ordered motion characterizes LSCI measurement in large vessels. Table 3.2 shows the field correlation function with respect to the region of CBF measurement.

g_1 model	Blood flow region
$exp(-\sqrt{\tau/\tau_c})$	Parenchyma
$exp(-\tau/\tau_c)$	Mid-sized vessel
$exp[-(\tau/\tau_c)^2]$	Large vessel

Table 3.2: Field correlation function with respect to the region of blood flow.

Chapter 4

New speckle contrast models: LSCI measurement in brain parenchyma and large vessels

To make LSCI a quantitative tool for blood flow measurement, the proper contrast model which links the speckle contrast to the blood flow is supposed to be used depending on the location of the blood flow. Based on the region of blood flow, the correct form of field correlation function should be used with the static scattering effect and the value of the coherence factor taken into account. The appropriate contrast equation $MO/SU_{n=1}$ for flow measurement in mid-sized vessels has been derived in (Parthasarathy et al., 2008) and is shown in Eq. (3.5). Here we derive the contrast models with the field correlation function $MU_{n=0.5}$ and $SO_{n=2}$, which are supposed to be applied for flow measurement in brain parenchyma and large vessels.

The field correlation function used for CBF measurement in parenchyma is:

$$g_1(\tau) = exp(-\sqrt{\tau/\tau_c}) \tag{4.1}$$

Substitute Eq. (4.1), the modified Siegert relation Eq. (3.4), and Eq. (2.7) in Eq. (2.5), the new-derived contrast model for flow measurement in parenchyma is:

$$\begin{aligned} K = \beta^{1/2}\Bigg\{ & \rho^2 \frac{e^{-2\sqrt{x}}(4x + 6\sqrt{x} + 3) + 2x - 3}{2x^2} \\ & + 8\rho(1-\rho)\frac{e^{-\sqrt{x}}(2x + 6\sqrt{x} + 6) + x - 6}{x^2} + (1-\rho)^2 \Bigg\}^{1/2} \end{aligned} \tag{4.2}$$

where $x = T/\tau_c$.

The field correlation function for CBF measurement in large vessels is:

$$g_1(\tau) = exp\big[-(\tau/\tau_c)^2\big] \tag{4.3}$$

Substitute the Eq. (4.3), the modified Siegert relation Eq. (3.4) and Eq. (2.7) in Eq. (2.5), the speckle contrast equation for flow measurement in large vessels is

$$\begin{aligned} K = \beta^{1/2}\Big\{\rho^2 \frac{e^{-2x^2} + \sqrt{2\pi}erf(\sqrt{2}x)x - 1}{2x^2} \\ + 2\rho(1-\rho)\frac{e^{-x^2} + \sqrt{\pi}erf(x)x - 1}{x^2} + (1-\rho)^2\Big\}^{1/2} \end{aligned} \tag{4.4}$$

The details about the derivation are shown in Appendix. Figure 4·1 shows the contrast versus τ_c/T curves of four speckle contrast models. The dynamic component ρ and the β value are ones when plotting the curves.

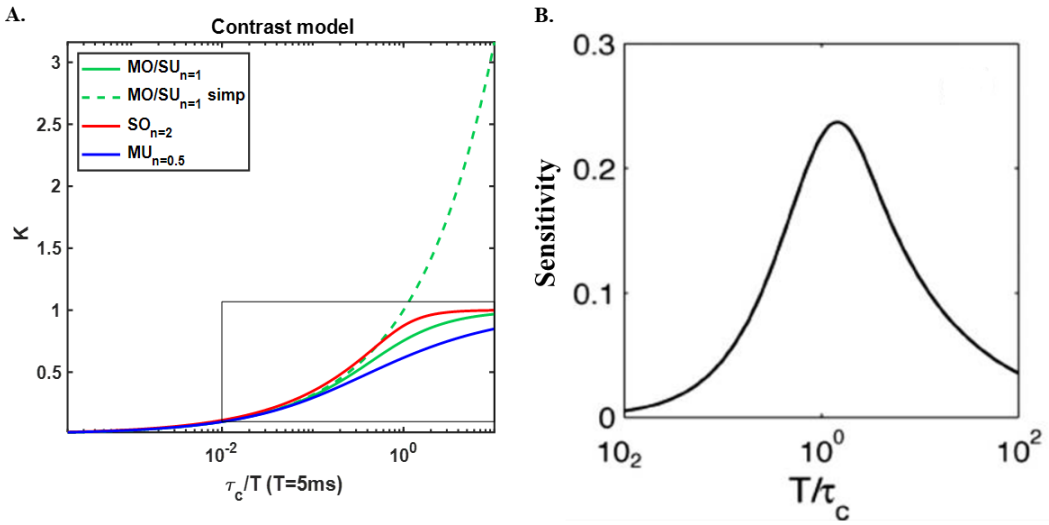

Figure 4·1: (A) Speckle contrast models with different field correlation function assumptions. $T = 5ms$. (B) Speckle contrast sensitivity to particle dynamics (Yuan et al., 2005; Boas and Dunn, 2010)

Based on the previous study, the speckle contrast is only sensitive to the particle dynamics within the range of T/τ_c from 10^{-2} to 10^2 (Figure 4·1 (B)). That means the speckle contrast models only function in the small box in Figure 4·1 (A). For fast flow measurement (i.e., τ_c/T less than 10^{-2}), the speckle contrast cannot give a robust estimation of the particle dynamics such that the form of contrast model is trivial. In contrast, as τ_c/T increases, apparent differences can be observed for the contrast estimated via different contrast models. Therefore, it is important to apply correct contrast models for slow flow measurement.

Chapter 5

Methods

5.1 Computational simulation

Computational simulation was utilized to quantify the flaws in modern laser speckle contrast theory. Initialize the true relative cerebral blood flow ($rCBF_t$) and using speckle contrast model with the wrong assumptions to obtain the measured $rCBF_m$. The error resulting from the wrong contrast model is quantified using relative error (RE) which is defined as:

$$Relative\ error = \frac{rCBF_m - rCBF_t}{rCBF_t} \times 100\% \tag{5.1}$$

In the simulation process, the baseline blood flow in large vessel, mid-sized vessel, and the brain parenchyma was simulated by initializing the baseline correlation time as $50\mu s$, $200\mu s$ and $1ms$. We tested the influence of different LSCI assumptions on rCBF between 10% (stroke) to 300% (hypercapnia) of the baseline. The exposure time used during the simulation is $5ms$. After initializing the baseline correlation time and the relative flow, the response correlation time can be obtained from the ratio of baseline correlation time to the relative flow. The correct contrast model (i.e., contrast model with right assumptions on the field correlation function, static scattering effect, and the coherence factor) was used to calculate the baseline and the response contrast. The contrast values were put into the wrong contrast model (i.e., contrast model with wrong assumptions) to get the measured correlation time

and the measured relative flow ($rCBF_m$). The flowchart of the simulation process is illustrated in Figure 5·1.

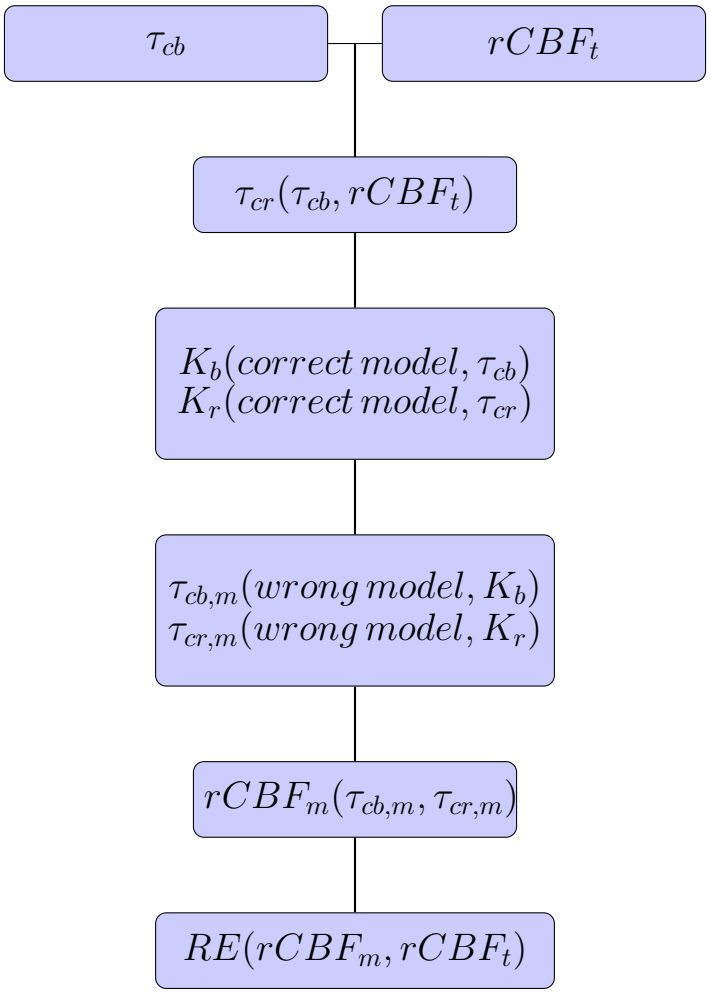

Figure 5·1: Flowchart of computational simulation. τ_{cb}: baseline correlation time; τ_{cr}: response correlation time; K_b: baseline contrast; K_r: response contrast; $\tau_{cb,m}$: measured baseline correlation time; $\tau_{cr,m}$: measured response correlation time; $rCBF_t$: true rCBF; $rCBF_m$: measured rCBF; RE: relative error.

5.2 Animal experiment

5.2.1 Animal preparation and stimuli type

All animal procedures were approved by the Boston University Institutional Animal Care and Use Committee and were conducted following the Guide for the Care and Use of Laboratory Animals. Anesthetized Mice (female, 25g, wild type C57BL/6, n=1) with isoflurane (3% induction, $1 - 1.5\%$ maintenance) and placed it on the stereotaxic frame. Temperature was maintained at $37°C$ with a homeothermic blanket. A cranial window was created to achieve better image quality.

CO_2 induced hypercapnia was applied to test the LSCI performance on measuring the increased blood flow. The breath air for the mouse was provided by two gas cylinders ($5\%CO_2/AI$, Airgas, USA and OX USP300, Airgas, USA). Two flowmeters were used to adjust the concentration of CO_2 in the breath air. The fraction of CO_2 was adjusted from 0% at baseline to 1.25%, 2.5%, and 3.75% to trigger CBF increase.

Carotid artery ligation was performed to accomplish hypoperfusion for testing the LSCI performance on measuring decreased blood flow. One of the carotid arteries was ligated with threads to trigger initial blood flow reduction, the other carotid artery was ligated afterward to induce further reduction of CBF.

5.2.2 LSCI measurement

A VHG-stabilized laser diode (785nm, LD785-SEV300, Thorlabs, USA) illuminated light into the skull. The light collimated with an optical isolator (IO-5-780-VLP, Thorlabs, USA) passed through an anamorphic prism pair (PS875-B-N-SF11, Thorlabs, USA) and was expanded by an expander (GBE10-B-10X, Thorlabs, USA). The backscattered light transmitted into a $\times 5$ objective with $NA = 0.14$ (Mitutoyo, Japan) and was captured using a high-speed camera (Fastec IL5-S, 1280×1024 pixels, 991 fps, $5\mu m$ pixel size, Fastec, USA). The exposure time was adjusted to $5ms$

for LSCI measurement. A region of interest (ROI) (1024×150 pixels) was selected for CBF measurement during baseline, hypercapnia, and carotid artery ligation. The speckle contrast images were averaged over $4s$ to reduce the noise. To estimate the rCBF in large vessels, mid-sized vessels and parenchyma, the speckle contrast images were masked based on the intensity to identify different regions, and the rCBF was estimated using the simplified speckle contrast model. Eventually, rCBF in each type of regions were averaged over all corresponding pixels to keep the statistics fidelity.

5.2.3 Dynamic laser speckle imaging (DLSI) measurement

Dynamic laser speckle imaging (DLSI) was used to provide a ground truth of the rCBF for validating modern LSCI measurement. The exposure time was shorten to $31\mu s$ for blood flow measurement of the same ROI during normal condition, hypercapnia and hypoperfusion. With the short exposure time, DLSI measures the fluctuations of the intensity by calculating the intensity correlation function g_2. The intensity correlation curve is fitted through the relation between g_2 to the field correlation function to get the correlation time. In the experiment, $g_2(\tau)$ of each pixel was calculated over $4s$. Since the fitting process is computationally expensive, we simplified the computation by linear interpolation. g_2 value at time $t = 0$ and $t = \tau_c$ can be derived via the Siegert relation:

$$g_2(0) = 1 + \beta|g_1(0)|^2 \tag{5.2}$$

$$g_2(\tau_c) = 1 + \beta|g_1(\tau_c)|^2 \tag{5.3}$$

The field correlation function is one at time $t = 0$ and is $1/e$ at time $t = \tau_c$ whatever the form of field correlation function is. Hence we have:

$$\begin{aligned} g_2(0) &= 1 + \beta \\ g_2(\tau_c) &= 1 + \frac{\beta}{e^2} \end{aligned} \tag{5.4}$$

The relation between $g_2(0)$ and $g_2(\tau_c)$ is:

$$g_2(\tau_c) = 1 + \frac{g_2(0) - 1}{e^2} \tag{5.5}$$

One can easily obtain the value of $g_2(0)$ and $g_2(\tau_c)$ and get the correlation time τ_c through linear interpolation. But since we used the Siegert relation, the static scattering was not considered. The correlation times of all pixels were averaged based on the region of blood flow. rCBF was calculated by the ratio of the baseline correlation time to the response correlation time. Note here applying the Siegert relation without static scattering modification might lead to measurement error. To achieve accurate flow measurement via DLSI, correct relation between the field correlation function and the intensity correlation function is supposed to be used (Postnov et al., 2019).

Chapter 6

Results

6.1 Impact of choosing wrong coherence factor β on relative flow measurement

Figure 6·1 shows that using wrong value of β underestimates flow change. The impact of the coherence factor is particularly obvious for relative flow measurement in parenchyma. We simulated ten conditions with the true β value (β_{true}) varying from 0.1 to 1. Contrast models with β_{true} were used to get the contrast values, which were converted into τ_c using the contrast model in which β equals to one. The static scattering is ignored in this test, and exposure time $T = 5ms$.

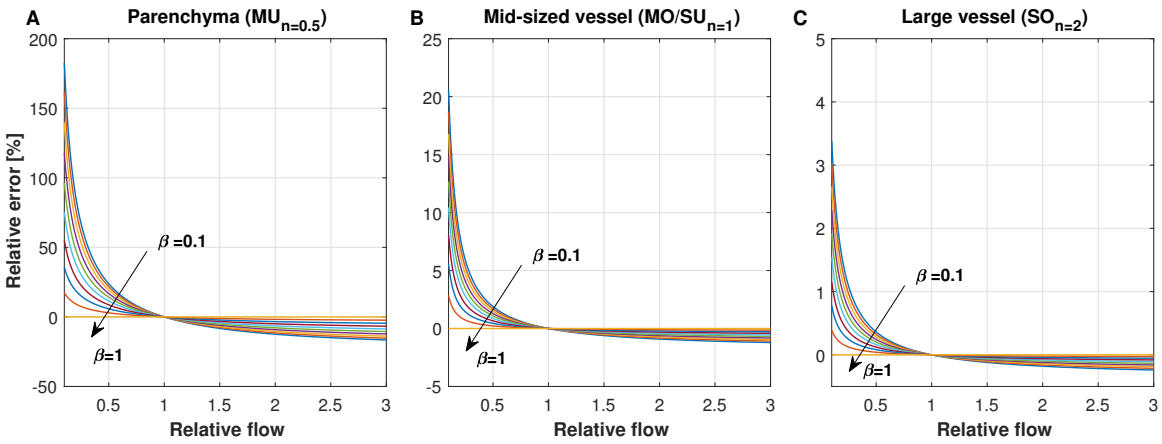

Figure 6·1: Impact of the coherence factor β on rCBF measurement in parenchyma (A), mid-sized vessels (B), and large vessels (C).

6.2 Impact of ignoring static scattering effect on relative flow measurement

In Figure 6·2, we tested the influence of ignoring static scattering ($\rho = 1$) on rCBF measurement under the conditions that the actual dynamic component ρ varies from 0.1 to 1, with the step 0.1. It turns out that ignoring static scattering would lead to relative flow underestimation. The error caused by the ignoring is pretty significant for relative flow in large vessels. Contrast models with the actual ρ value were used to calculate the contrasts, which were converted into the correlation time using the contrast model that ignores the static scattering effect. rCBF was calculated by the ratio of the baseline correlation time to the response correlation time. Relative error was calculated using Eq. (5.1). Coherence factor $\beta = 1$ for both contrast and relative flow computation, exposure time $T = 5ms$.

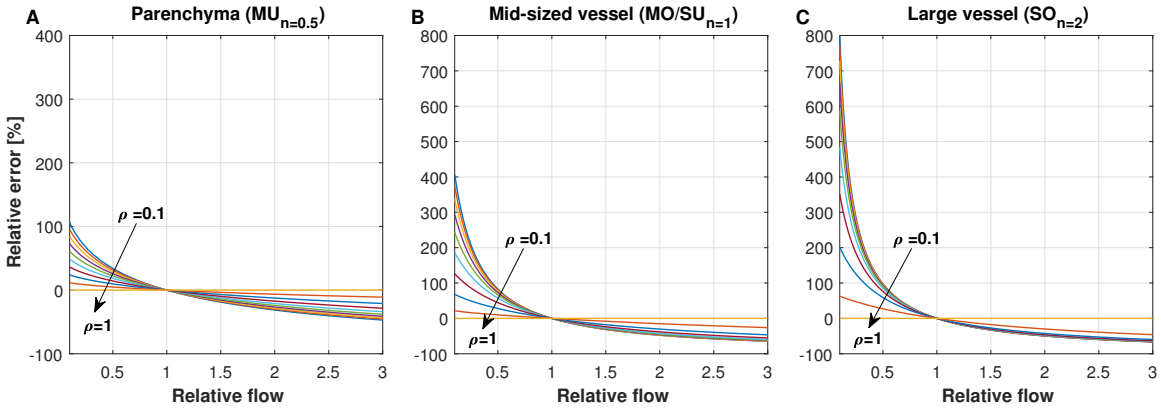

Figure 6·2: Impact of static scattering on rCBF measurement in parenchyma (A), mid-sized vessels (B), and large vessels (C).

6.3 Consequence of assuming wrong form of field correlation function

Based on what has been discussed, speckle contrast models with various forms of the field correlation function should be used for measuring relative flow in different

regions. Modern LSCI method is only proper to rCBF measurement in mid-sized vessels. Figure 6·3 demonstrates that the misuse of modern LSCI analysis in the rCBF measurement of brain parenchyma leads to the overestimated rCBF during CBF reduction and the underestimated rCBF during CBF increase, while the relative error caused by the wrong contrast model for rCBF measurement in the large vessel is negligible. The correct contrast model for parenchyma ($MU_{n=0.5}$), mid-sized vessels ($MO/SU_{n=1}$) and large vessels ($SO_{n=2}$) were used to calculate the speckle contrasts. The speckle contrasts were converted into the correlation time using modern LSCI model to obtain the measurement result of rCBF. Relative error was calculated using Eq. (5.1) to compare the measured rCBF with the pre-assumed true rCBF. Static scattering was ignored in the simulation. Coherence factor $\beta = 1$, exposure time $T = 5ms$.

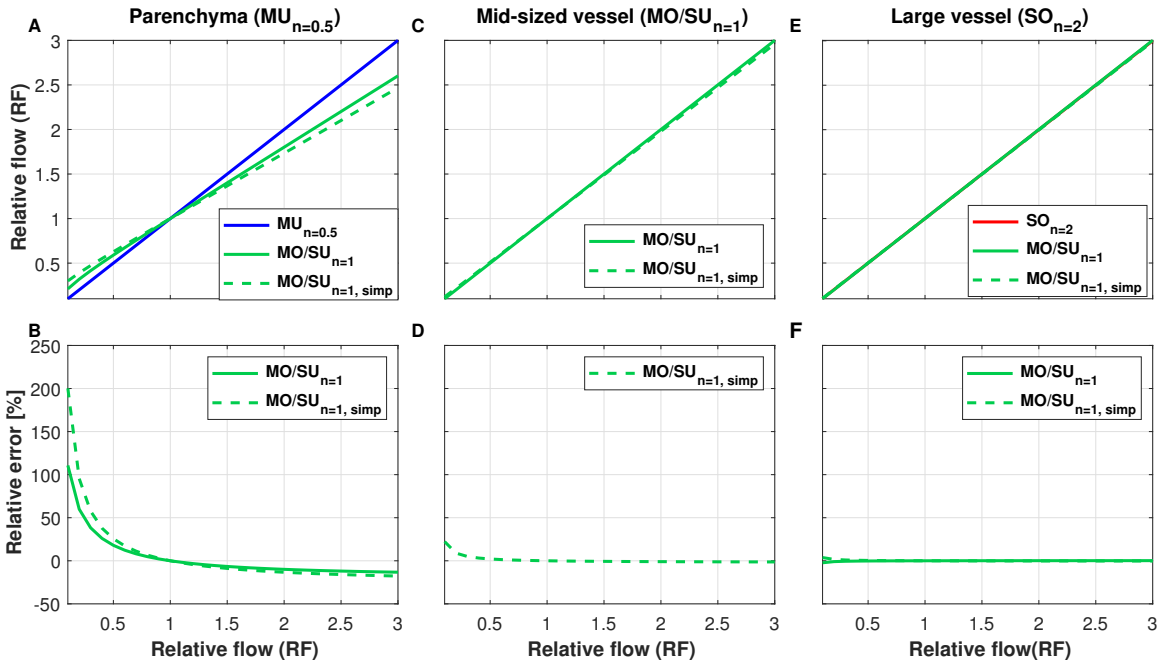

Figure 6·3: (A, C, E) Comparison of rCBF measured by the correct contrast model and the modern LSCI model. (B,D,F) Relative error of rCBF measurement caused by modern LSCI model.

6.4 Modern LSCI underestimates the flow change

Figure 6·4 presents the mouse rCBF of the region of interest measured by both LSCI and DLSI during hypercapnia and carotid artery ligation. As it turns out, modern LSCI underestimates the rCBF during CBF increase ($rCBF > 1$) and overestimates the rCBF during CBF decrease ($rCBF < 1$). Figure 6·4 (B) is an image mask that was applied to identify pixels that belong to large vessel, mid-sized vessel or parenchyma. The blood flow in each "vessel type" were averaged over all corresponding pixels. The experiment result is consistent with the simulation result shown in Figure 6·3 (A, C, E) , which supports the idea that modern LSCI method underestimates blood flow change. Note that the result of relative flow in mid-sized vessel is almost the same with that in the parenchyma region, which might due to the inappropriate fitting of the $g_2(\tau)$ function.

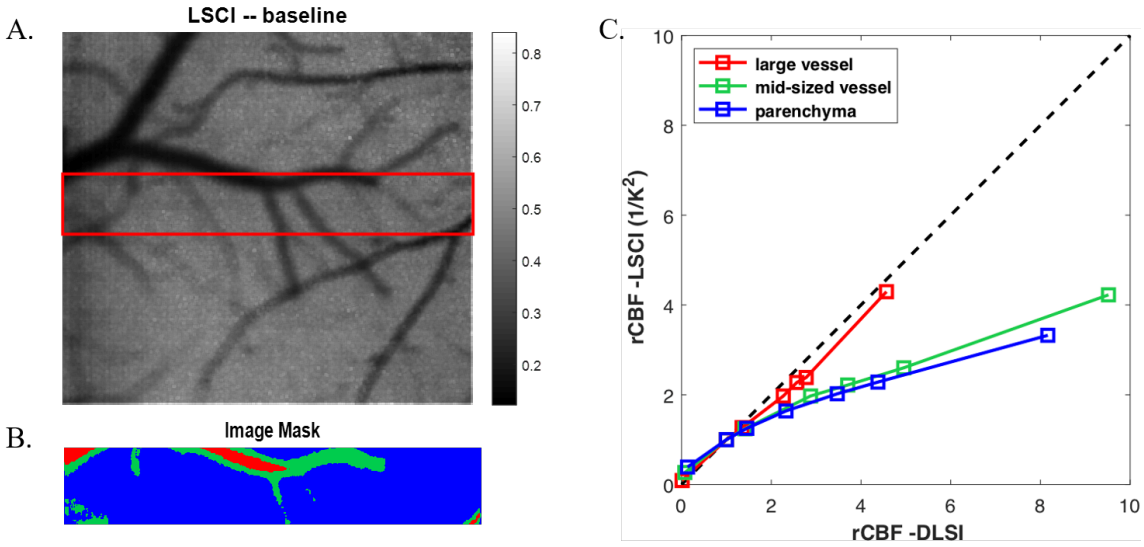

Figure 6·4: (A) Baseline speckle contrast image of the mouse brain with the ROI circled by red lines. (B) Image mask used for identifying different CBF regions. (C) Comparison of the rCBF measured by LSCI to DLSI.

Chapter 7

Discussion

7.1 Modern LSCI theory malfunctions for slow blood flow measurement

According to the rCBF estimation results obtained from the computational simulation (Figure 6·3) and the animal experiment (Figure 6·4), modern LSCI (the simplified model) underestimates the blood flow change. The relative error in relative blood flow is particularly obvious for slow blood flow measurement. Figure 4·1 presented that the performances of the speckle contrast models are highly dependent on the ratio of τ_c to T: the contrast values estimated by various models are less different from each other as τ_c goes shorter, especially for super fast flow measurement ($\tau_c << T$) in which situation that the contrast is less sensitive to the blood flow; while the differences between the contrasts from different models become more and more significant as τ_c goes towards to T. For relative blood flow measurement in large vessels and mid-sized vessels where the correlation time is short, using the wrong contrast model (modern LSCI) won't affect the relative blood flow measurement significantly (Figure 6·3 (C-E)). However, for relative flow measurement in parenchyma in which blood flow is slow and the correlation time is long, modern LSCI could cause large relative error for relative blood flow measurement (Figure 6·3 (A, B)).

7.2 Choosing the wrong β affects relative blood flow measurement for the slow blood flow

As a factor that solely depends on the imaging system, it is interesting to see that the impact of β is different on the relative flow measurement in parenchyma, mid-sized vessels, and large vessels (Figure 6·1). For large vessels, the blood flow is fast and the correlation time is regraded as much shorter than the exposure time, so that the contrast model with $MO/SU_{n=1}$ can be simplified. When using the simplified model for relative flow estimation, β is removed so it won't affect the measurement. Therefore, the relative error caused by using the wrong β is negligible for relative flow measurement in large vessel (Figure 6·1 (C)). Whereas for relative flow measurement in mid-sized vessels and in the parenchyma, the contrast models cannot be simplified because of the long correlation time. As a result, β plays an important role in the relative flow estimation and using the wrong value would lead to high measurement error.

7.3 Static scattering affects relative flow measurement for the fast blood flow

In Figure 6·2, ignoring static scattering (i.e., $\rho = 1$) overestimates the rCBF during flow decrease (rCBF< 1) and underestimates the rCBF during flow increase (rCBF$>$ 1). In other words, the blood flow change is underestimated. It is interesting to notice that the impact of static scattering effect is different in the three contrast models. The inconsistent performance of static scattering on different contrast models (or the region where blood flow is measured) might because (1) the mathematical relation between the static scattering effect (i.e., the dynamic component ρ) and the speckle contrast is different based on the form of field correlation function; (2) the effect of static scattering might influenced by the speed of blood flow. Ignoring static

scattering brings more relative error for relative blood flow measurement in large vessels (where the $SO_{n=2}$ model is correct) as compared to the mid-sized vessels, which is in its turn results in larger error compared to parenchyma. This suggests that multiple exposure speckle imaging (MESI), which assumes the $MO/SU_{n=1}$ model everywhere, overestimates the static scattering effect in parenchyma region. To avoid the static scattering effect for cerebral blood measurement in large vessels, the skull is usually thinned or removed, while for the experiments performed without thinning the skull, one should consider the possibility of static scattering strongly affecting the relative flow in large vessels.

Chapter 8

Conclusions

The simplified contrast model used in modern LSCI measurement allows the fast acquisition of the relative blood flow. However, the model underestimates the flow change. The measurement imprecision is particular obvious when measuring slow blood flow, for example, CBF in brain parenchyma. The imprecision of modern LSCI is due to the wrong assumption of the field correlation function, the ignoring of static scattering and the coherence factor. To improve the LSCI measurement, speckle contrast model with the correct field correlation function, and the correct value of the dynamic component and the coherence factor is suggested when measuring slow blood flow; while for blood flow measurement in large vessels, the simplified contrast model is still feasible and technically benefits the blood flow measurement.

Appendix A

Speckle Contrast model derivation

A.1 Contrast model with the field correlation function $SO_n = 2$

The speckle contrast equation considering static scattering is:

$$K^2 = \frac{2\beta}{T}\int_0^T (1-\frac{\tau}{T})\big[\rho^2 g_1(\tau)^2 + 2\rho(1-\rho)g_1(\tau) + (1-\rho)^2\big]d\tau \tag{A.1}$$

The field correlation function corresponding to single scattering and ordered motion (large vessel)is:

$$g_1(\tau) = exp\big[-\big(\frac{\tau}{\tau_c}\big)^2\big] \tag{A.2}$$

Substitute Eq. (A.2) into Eq. (A.1) we have:

$$\begin{aligned} K^2 =& \frac{2\beta}{T}\int_0^T (1-\frac{\tau}{T})\Big\{\rho^2 exp\big[-\big(\frac{\tau}{\tau_c}\big)^2\big]^2 + 2\rho(1-\rho)exp[-\big(\frac{\tau}{\tau_c}\big)^2] \\ &+ (1-\rho)^2\Big\}d\tau \end{aligned} \tag{A.3}$$

Then we calculate the integration:

$$
\begin{aligned}
K^2 =& \frac{2\beta}{T}\Big\{\rho^2\frac{\sqrt{2\pi}}{4}\tau_c erf(\sqrt{2}\frac{\tau}{\tau_c})\Big|_0^T + 2\rho(1-\rho)\frac{\sqrt{\pi}}{2}\tau_c erf(\frac{\tau}{\tau_c})\Big|_0^T + (1-\rho)^2\Big|_0^T \\
& - \frac{1}{T}\Big\{-\rho^2\frac{\tau_c^2}{4}exp[-(\frac{2\tau^2}{\tau_c^2})]\Big|_0^T - 2\rho(1-\rho)\frac{\tau_c^2}{2}exp[-(\frac{\tau}{\tau_c})^2]\Big|_0^T + \tau(1-\rho)^2\Big|_0^T\Big\}\Big\} \\
=& \frac{2\beta}{T}\Big\{\rho^2\frac{\sqrt{2\pi}}{4}\tau_c erf(\sqrt{2}\frac{T}{\tau_c}) + 2\rho(1-\rho)\frac{\sqrt{\pi}}{2}\tau_c erf(\frac{T}{\tau_c}) + T(1-\rho)^2 \\
& - \frac{1}{T}\Big\{-\rho^2\frac{\tau_c^2}{4}\big\{exp[-(\frac{2T^2}{\tau_c^2})]-1\big\} - 2\rho(1-\rho)\frac{\tau_c^2}{2}\big\{exp[-(\frac{T}{\tau_c})^2]-1\big\} \\
& + \frac{T^2}{2}(1-\rho)^2\Big\}\Big\}
\end{aligned}
\tag{A.4}
$$

Reorganize Eq. (A.4) and use $x = T/\tau_c$, the contrast equation with the field correlation function $SO_{n=2}$ can be represented as:

$$
\begin{aligned}
K =& \beta^{1/2}\Big\{\rho^2\frac{e^{-2x^2} + \sqrt{2\pi}erf(\sqrt{2}x)x - 1}{2x^2} \\
& + 2\rho(1-\rho)\frac{e^{-x^2} + \sqrt{\pi}erf(x)x - 1}{x^2} + (1-\rho)^2\Big\}^{1/2}
\end{aligned}
\tag{A.5}
$$

A.2 Contrast model with the field correlation function $MU_n = 0.5$

The field correlation function corresponding to multiple scattering and unordered motion (parenchyma) is:

$$
g_1(\tau) = exp\Big(-\sqrt{\frac{\tau}{\tau_c}}\Big) \tag{A.6}
$$

Substitute Eq. (A.6) into Eq. (A.1), we have

$$
K^2 = \frac{2\beta}{T}\int_0^T (1-\frac{\tau}{T})\Big\{\rho^2 exp\big(-\sqrt{\frac{\tau}{\tau_c}}\big)^2 + 2\rho(1-\rho)exp\big(-\sqrt{\frac{\tau}{\tau_c}}\big) + (1-\rho)^2\Big\}d\tau \tag{A.7}
$$

The Eq. (A.7) can be further computed as:

$$\begin{aligned}K^2 =&\frac{2\beta}{T}\Big\{ -\rho^2\frac{\tau_c}{2}exp(-2\sqrt{\frac{\tau}{\tau_c}})(2\sqrt{\frac{\tau}{\tau_c}}+1)\Big|_0^T \\ &-4\rho(1-\rho)\tau_c exp(-\sqrt{\frac{\tau}{\tau_c}})(\sqrt{\frac{\tau}{\tau_c}}+1)\Big|_0^T+(1-\rho)^2\Big|_0^T \\ &-\frac{1}{T}\Big\{ -\rho^2\frac{\tau_c}{4}exp(-2\sqrt{\frac{\tau}{\tau_c}})(4\tau\sqrt{\frac{\tau}{\tau_c}}+6\tau_c\sqrt{\frac{\tau}{\tau_c}}+6\tau+3\tau_c)\Big|_0^T \\ &-4\rho(1-\rho)\tau_c exp(-\sqrt{\frac{\tau}{\tau_c}})\Big[\tau(\sqrt{\frac{\tau}{\tau_c}}+3)+6\tau_c(\sqrt{\frac{\tau}{\tau_c}}+1)\Big]\Big|_0^T+\tau(1-\rho)^2\Big|_0^T\Big\}\Big\}\end{aligned} \tag{A.8}$$

substitute $x = T/\tau_c$ in Eq. (A.8), the contrast equation with the field correlation function $MU_{n=0.5}$ is:

$$\begin{aligned}K =&\beta^{1/2}\Big\{\rho^2\frac{e^{-2\sqrt{x}}(4x+6\sqrt{x}+3)+2x-3}{2x^2} \\ &+8\rho(1-\rho)\frac{e^{-\sqrt{x}}(2x+6\sqrt{x}+6)+x-6}{x^2}+(1-\rho)^2\Big\}^{1/2}\end{aligned} \tag{A.9}$$

Note that the noise effect on contrast calculation is ignored.

References

Ansari, M. and Nirala, A. (2015). Monitoring capillary blood flow using laser speckle contrast analysis with spatial and temporal statistics. *Optik*, 126(24):5224 – 5229.

Bandyopadhyay, R., Gittings, A., Suh, S., Dixon, P., and Durian, D. J. (2005). Speckle-visibility spectroscopy: A tool to study time-varying dynamics. *Review of scientific instruments*, 76(9):093110.

Boas, D. A. and Dunn, A. K. (2010). Laser speckle contrast imaging in biomedical optics. *Journal of biomedical optics*, 15(1):011109.

Briers, J. D. (2001). Laser doppler, speckle and related techniques for blood perfusion mapping and imaging. *Physiological measurement*, 22(4):R35.

Briers, J. D. and Webster, S. (1996). Laser speckle contrast analysis (lasca): a nonscanning, full-field technique for monitoring capillary blood flow. *Journal of biomedical optics*, 1(2):174–180.

Buckley, E. M., Parthasarathy, A. B., Grant, P. E., Yodh, A. G., and Franceschini, M. A. (2014). Diffuse correlation spectroscopy for measurement of cerebral blood flow: future prospects. *Neurophotonics*, 1(1):011009.

Cheng, H. and Duong, T. Q. (2007). Simplified laser-speckle-imaging analysis method and its application to retinal blood flow imaging. *Optics letters*, 32(15):2188–2190.

Cheng, H., Luo, Q., Zeng, S., Chen, S., Cen, J., and Gong, H. (2003). Modified laser speckle imaging method with improved spatial resolution. *Journal of Biomedical Optics*, 8(3):559–565.

Choi, B., Kang, N. M., and Nelson, J. S. (2004). Laser speckle imaging for monitoring blood flow dynamics in the in vivo rodent dorsal skin fold model. *Microvascular Research*, 68(2):143–146.

Davis, M. A., Gagnon, L., Boas, D. A., and Dunn, A. K. (2016). Sensitivity of laser speckle contrast imaging to flow perturbations in the cortex. *Biomedical optics express*, 7(3):759–775.

Davis, M. A., Kazmi, S. S., and Dunn, A. K. (2014). Imaging depth and multiple scattering in laser speckle contrast imaging. *Journal of biomedical optics*, 19(8):086001.

Dirnagl, U., Kaplan, B., Jacewicz, M., and Pulsinelli, W. (1989). Continuous measurement of cerebral cortical blood flow by laserdoppler flowmetry in a rat stroke model. *Journal of Cerebral Blood Flow & Metabolism*, 9(5):589–596. PMID: 2674168.

Duncan, D. D. and Kirkpatrick, S. J. (2008). Can laser speckle flowmetry be made a quantitative tool? *JOSA A*, 25(8):2088–2094.

Dunn, A. K., Bolay, H., Moskowitz, M. A., and Boas, D. A. (2001). Dynamic imaging of cerebral blood flow using laser speckle. *Journal of Cerebral Blood Flow & Metabolism*, 21(3):195–201.

Durduran, T. and Yodh, A. G. (2014). Diffuse correlation spectroscopy for noninvasive, micro-vascular cerebral blood flow measurement. *Neuroimage*, 85:51–63.

Fercher, A. and Briers, J. D. (1981). Flow visualization by means of single-exposure speckle photography. *Optics communications*, 37(5):326–330.

Fredriksson, I., Fors, C., and Johansson, J. (2007). Laser doppler flowmetry-a theoretical framework. *Department of Biomedical Engineering, Linköping University*, pages 6–7.

Hecht, N., Müller, M.-M., Sandow, N., Pinczolits, A., Vajkoczy, P., and Woitzik, J. (2016). Infarct prediction by intraoperative laser speckle imaging in patients with malignant hemispheric stroke. *Journal of Cerebral Blood Flow & Metabolism*, 36(6):1022–1032.

Huang, Y.-C., L.Ringold, T., Nelson, S., and Choi, B. (2008). Noninvasive blood flow imaging for real-time feedback during laser therapy of port wine stain birthmarks. *Lasers in surgery and medicine*, 40(3):167–173.

Kazmi, S. S., Faraji, E., Davis, M. A., Huang, Y.-Y., Zhang, X. J., and Dunn, A. K. (2015). Flux or speed? examining speckle contrast imaging of vascular flows. *Biomedical optics express*, 6(7):2588–2608.

Kirkpatrick, S. J., Duncan, D. D., and Wells-Gray, E. M. (2008). Detrimental effects of speckle-pixel size matching in laser speckle contrast imaging. *Optics letters*, 33(24):2886–2888.

Lemieux, P.-A. and Durian, D. (1999). Investigating non-gaussian scattering processes by using nth-order intensity correlation functions. *JOSA A*, 16(7):1651–1664.

Li, Y., Zhu, S., Yuan, L., Lu, H., Li, H., and Tong, S. (2013). Predicting the ischemic infarct volume at the first minute after occlusion in rodent stroke model by laser speckle imaging of cerebral blood flow. *Journal of biomedical optics*, 18(7):076024.

Liu, C., Xie, B., Li, M., Yang, G.-y., and Tong, S. (2011). Spatiotemporal changes of cerebral blood flow following hemorrhagic stroke by laser speckle imaging. In *2011 Annual International Conference of the IEEE Engineering in Medicine and Biology Society*, pages 6150–6153. IEEE.

Liu, Q., Chen, S., Soetikno, B., Liu, W., Tong, S., and Zhang, H. F. (2018). Monitoring acute stroke in mouse model using laser speckle imaging-guided visible-light optical coherence tomography. *IEEE Transactions on Biomedical Engineering*, 65(10):2136–2142.

Nakamura, H., Strong, A. J., Dohmen, C., Sakowitz, O. W., Vollmar, S., Sue, M., Kracht, L., Hashemi, P., Bhatia, R., Yoshimine, T., et al. (2010). Spreading depolarizations cycle around and enlarge focal ischaemic brain lesions. *Brain*, 133(7):1994–2006.

Parthasarathy, A. B., Tom, W. J., Gopal, A., Zhang, X., and Dunn, A. K. (2008). Robust flow measurement with multi-exposure speckle imaging. *Optics express*, 16(3):1975–1989.

Postnov, D. D., Erdener, E. S., Tang, J., Kilic, K., and Boas, D. A. (2019). Dynamic laser speckle imaging. *Manuscript in preparation*.

Qiu, J., Li, P., Luo, W., Wang, J., Zhang, H., and Luo, Q. (2010). Spatiotemporal laser speckle contrast analysis for blood flow imaging with maximized speckle contrast. *Journal of biomedical optics*, 15(1):016003.

Ramirez-San-Juan, J. C., Ramos-Garcia, R., Guizar-Iturbide, I., Martinez-Niconoff, G., and Choi, B. (2008). Impact of velocity distribution assumption on simplified laser speckle imaging equation. *Optics express*, 16(5):3197–3203.

Roustit, M., Millet, C., Blaise, S., Dufournet, B., and Cracowski, J. (2010). Excellent reproducibility of laser speckle contrast imaging to assess skin microvascular reactivity. *Microvascular research*, 80(3):505–511.

Senarathna, J., Rege, A., Li, N., and Thakor, N. V. (2013). Laser speckle contrast imaging: theory, instrumentation and applications. *IEEE reviews in biomedical engineering*, 6:99–110.

Serov, A. and Lasser, T. (2005). High-speed laser doppler perfusion imaging using an integrating cmos image sensor. *Optics Express*, 13(17):6416–6428.

Shin, H. K., Dunn, A. K., Jones, P. B., Boas, D. A., Moskowitz, M. A., and Ayata, C. (2006). Vasoconstrictive neurovascular coupling during focal ischemic depolarizations. *Journal of Cerebral Blood Flow & Metabolism*, 26(8):1018–1030.

Srienc, A. I., Kurth-Nelson, Z. L., and Newman, E. (2010). Imaging retinal blood flow with laser speckle flowmetry. *Frontiers in neuroenergetics*, 2:128.

Yuan, S., Devor, A., Boas, D. A., and Dunn, A. K. (2005). Determination of optimal exposure time for imaging of blood flow changes with laser speckle contrast imaging. *Applied optics*, 44(10):1823–1830.

CURRICULUM VITAE